

# Optical Engineering

[SPIDigitalLibrary.org/oe](http://SPIDigitalLibrary.org/oe)

## **Grouping design method with real ray tracing model for extreme ultraviolet lithographic objective**

Zhen Cao  
Yanqiu Li  
Fei Liu

# Grouping design method with real ray tracing model for extreme ultraviolet lithographic objective

Zhen Cao

Yanqiu Li

Fei Liu

Beijing Institute of Technology

School of Optoelectronics

Key Laboratory of Photoelectronic Imaging

Technology and System of Ministry of

Education of China

Beijing 100081, China

E-mail: [liyanqiu@bit.edu.com](mailto:liyanqiu@bit.edu.com)

**Abstract.** Choosing an adequate initial design for optimization plays an important role in obtaining high-quality extreme ultraviolet (EUV) lithographic objectives. A grouping design method with real ray tracing model is developed to acquire initial configurations of high numerical aperture (NA) objective for EUV lithography. In this method, the objective system is first divided into three mirror groups. The initial parameters of each mirror group are then determined by real ray calculation under design constraints. Finally, the three mirror groups are connected directly into a feasible initial system. Due to real ray calculation, the discrepancy of the ray path induced by paraxial approximation and the exhaustive search of variables is avoided in a high-NA objective design. In addition, the incidence angles on reflective mirrors can be controlled in the design of each group, which makes the initial configuration suited to further optimization and compatible multilayer design. An NA 0.33 six-mirror EUV lithographic objective is designed as an example to implement this method. © The Authors. Published by SPIE under a Creative Commons Attribution 3.0 Unported License. Distribution or reproduction of this work in whole or in part requires full attribution of the original publication, including its DOI. [DOI: [10.1117/1.OE.52.12.125102](https://doi.org/10.1117/1.OE.52.12.125102)]

Subject terms: grouping design method; optical design; extreme ultraviolet lithography; lithographic objective; optical system.

Paper 131224 received Aug. 8, 2013; revised manuscript received Oct. 31, 2013; accepted for publication Nov. 11, 2013; published online Dec. 16, 2013.

## 1 Introduction

Extreme ultraviolet (EUV) lithography is a promising candidate for next-generation lithography, so the design of an EUV lithographic objective system has received much attention in recent years.<sup>1-5</sup> For an EUV objective system, the large number of variables and design requirements make the optical system design difficult. In the past, several design methods for the initial configurations of EUV lithographic objective have been proposed in the literature. Lerner et al. applied  $y - \bar{y}$  design diagram to obtain initial solutions.<sup>6</sup> However, the applicability of this method to the objective systems, which have more than four reflective mirrors, requires further study. Bal et al. and Bociort et al. proposed a design method based on a paraxial approximation model and initial configurations were designed via exhaustive searching of all the independent variables.<sup>7,8</sup> Because the number of independent variables is large, the computation for a feasible initial configuration is very expensive and it is impossible to constrain the beam incidence angles on mirrors. Hudyma presented an idea of a grouping design for a six-mirror objective in which the objective was separated into two groups, but the design method was not mentioned.<sup>9</sup> Recently, we developed a grouping design method with paraxial analysis.<sup>10,11</sup> However, the paraxial approximation leads to the discrepancy of ray path and the mismatch for the pupils of three mirror groups. Thus an incorrect judgment for obstruction may have happened and the three mirror groups could not be connected directly to get a whole objective. We still have to make an iterative calculation and exhaustive search of variables to match the design constraints and to get a whole objective. In addition, although the adverse effects of large incidence angles on reflective mirrors

were demonstrated in a high-numerical aperture (NA) EUV objective system,<sup>12</sup> little attention has been paid to the control of incidence angles in the current initial configuration design methods.

In this paper, a grouping design method with real ray tracing model is developed to acquire spherical initial configurations of a six-mirror EUV objective. This is accomplished as follows: First, the whole system is divided into three mirror groups. Then the initial parameters of object-side group and image-side group are determined according to several aspects: requirements of objective design, design constraints such as aperture stop constraint, nonobstruction constraint, and incidence angle constraint. Once the parameters of object-side and image-side groups are determined, all the parameters of the middle group can be calculated with the conjugation constraint. Using a real ray tracing model, the pupils of three mirror groups are matched exactly. So the three mirror groups can be directly connected into a feasible objective system without iterative calculation and exhaustive search of variables when the middle group satisfies non-obstruction constraint and incidence angle constraint. In addition, some constraints imposed reduce the independent variables in an objective system, which significantly simplifies the design process. With this method, an NA 0.33 EUV lithographic objective is designed and a composite root-mean-square (RMS) wavefront error of  $0.026\lambda$  ( $\lambda = 13.5$  nm) is achieved through further optimization.

## 2 Grouping Design with Real Ray Tracing Model

In our grouping design strategy, an objective system is divided into object-side group (G1), middle group (G2), and image-side group (G3), and is shown in Fig. 1. Several

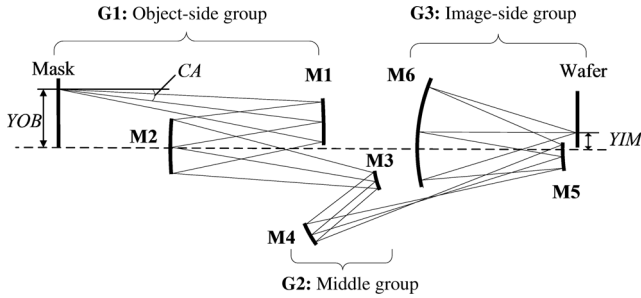


Fig. 1 Grouping strategy for a six-mirror EUV lithographic objective.

system parameters such as the NA on the image side and the magnification of system ( $M$ ) should be set according to the requirements of the objective design first. The image height ( $YIM$ ) and the chief ray angle of incidence on mask ( $CA$ ) are determined according to the following principles: The  $YIM$  should be adjusted appropriately to avoid obstruction on the fifth mirror  $M5$ , in order to avoid the intersection between the light cones of illuminator and objective and keep mask-induced effects small, so  $CA$  should be<sup>13</sup>

$$\arcsin(\text{NA} \times |M|) < CA \leq 6 \text{ deg}, \quad (1)$$

$$\text{NAO} = \text{NA} \times |M|, \quad (2)$$

$$\text{YOB} = \text{YIM}/|M|. \quad (3)$$

## 2.1 Object-Side Group

Object-side group ( $G1$ ) contains  $M1$  and  $M2$ . The configuration parameters of  $G1$  include the radius of  $M1$  ( $r_1$ ), the radius of  $M2$  ( $r_2$ ), the distance between mask and  $M1$  ( $L_1$ ), and the distance between  $M1$  and  $M2$  ( $d_1$ ). The ray path of  $G1$  is shown in Fig. 2.

A designer could assign reasonable values of  $L_1$  and  $d_1$  according to the limitation of beam incidence angle on  $M1$  and  $M2$  and total track of objective. To avoid obstruction, the clearance between the clear aperture of a mirror and the real ray beam nearby is determined by the edge region of a mirror and assembly requirement. The aperture stop of the objective system is placed on  $M2$ . According to the aperture stop constraint, the chief ray should pass through the center of the stop. Thus,  $r_1$  can be calculated by

$$r_1 = h_{z1} / \sin \left\{ \frac{CA}{2} - \frac{\arcsin \left[ \frac{h_{z1}}{-d_1 + z_{z1}} \right]}{2} \right\}, \quad (4)$$

where  $h_{z1}$  represents the chief ray height on  $M1$ , and  $z_{z1}$  represents the distance between the chief ray incidence point on

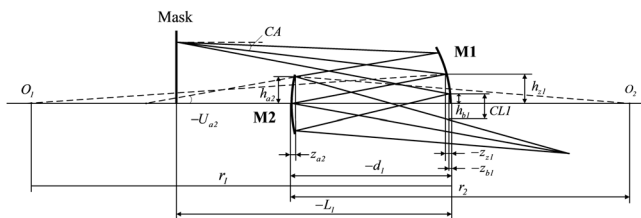


Fig. 2 Ray path of object-side group.

$M1$  and the vertex of  $M1$ . An aperture stop constraint can be used once, since there is only one stop in the objective system.

According to the nonobstruction constraint,  $r_2$  can be calculated by

$$r_2 = h_{a2} / \sin \left\{ \frac{U_{a2}}{2} + \frac{\arcsin \left[ \frac{(\text{CL1} - h_{b1} + h_{a2}) / (-d_1 - z_{a2} + z_{b1})}{2} \right]}{2} \right\}, \quad (5)$$

where  $\text{CL1}$  is the clearance mentioned above and it represents the longitudinal distance between the clear aperture of  $M1$  and the upper marginal ray reflected from  $M2$ ,  $h_{a2}$  represents the upper marginal ray height on  $M2$ ,  $h_{b1}$  represents the lower marginal ray height on  $M1$ ,  $U_{a2}$  represents the upper marginal ray aperture angle of  $M2$  on the object side,  $z_{a2}$  represents the distance between the upper marginal ray incidence point on  $M2$  and the vertex of  $M2$ , and  $z_{b1}$  represents the distance between the lower marginal ray incidence point on  $M1$  and the vertex of  $M1$ .

We first assign infinity to  $r_1$  and  $r_2$  as starting values. Then the unknown parameters ( $h_{z1}$ ,  $z_{z1}$ ,  $h_{a2}$ ,  $h_{b1}$ ,  $U_{a2}$ ,  $z_{a2}$ ,  $z_{b1}$ ) to calculate  $r_1$  and  $r_2$  in Eqs. (4) and (5) can be acquired by real ray tracing with the commercial optical design software CODE V. With the iterative computations, the results of  $r_1$  and  $r_2$  will be unchanged at last. In this way, all the parameters of  $G1$  are determined.

## 2.2 Image-Side Group

Image-side group ( $G3$ ) contains  $M5$  and  $M6$ . The chief ray is parallel to the optical axis on the wafer to meet a telecentricity condition. For convenience,  $G3$  is designed in a reverse sequence. The configuration parameters of  $G3$  include the radius of  $M5$  ( $r_5$ ), the radius of  $M6$  ( $r_6$ ), the distance between wafer and  $M6$  ( $L_6$ ), and the distance between  $M5$  and  $M6$  ( $d_5$ ). The ray path of  $G3$  is shown in Fig. 3.

The values of  $L_6$  and  $d_5$  are determined by the designer according to the total track requirement first. A virtual surface  $D1$  is then set at the position of  $M5$  and the incidence rays from the wafer pass through the virtual surface  $D1$  to  $M6$ . By imposing the nonobstruction constraint to  $M5$ ,  $r_6$  is calculated by

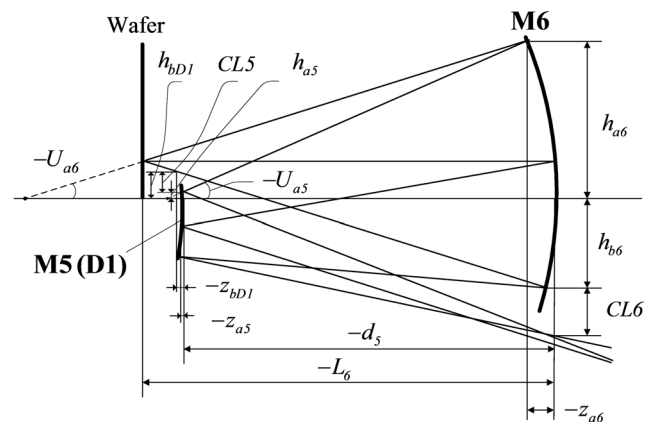


Fig. 3 Ray path of image-side group.

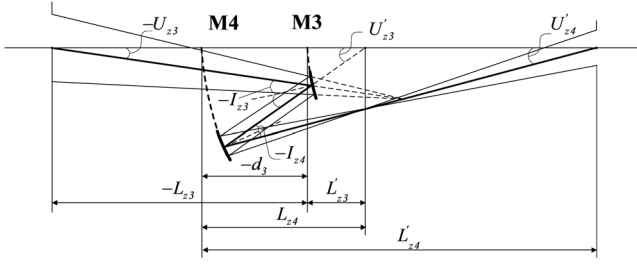


Fig. 4 Ray path of chief ray in middle group.

$$r_6 = h_{a6} / \sin \left\{ \frac{U_{a6}}{2} - \frac{\arctan[(CL5 - h_{bD1} + h_{a6}) / (-d_5 + z_{a6} - z_{bD1})]}{2} \right\}, \quad (6)$$

where  $h_{a6}$  represents the upper marginal ray height on M6,  $U_{a6}$  represents the upper marginal ray aperture angle of M6 on the object side, CL5 represents the longitudinal distance between the used area of M5 and the lower marginal ray passing through it,  $h_{bD1}$  represents the lower marginal ray height on D1,  $z_{a6}$  represents the distance between the upper marginal ray incidence point on M6 and the vertex of M6, and  $z_{bD1}$  represents the distance between the lower marginal ray incidence point on D1 and the vertex of D1. According to the nonobstruction constraint of M6,  $r_5$  is calculated by

$$r_5 = h_{a5} / \sin \left\{ \frac{U_{a5}}{2} + \frac{\arctan[(CL6 + h_{a5} + h_{b6}) / (-d_5 + z_{b6} - z_{a5})]}{2} \right\}, \quad (7)$$

where  $h_{a5}$  represents the upper marginal ray height on M5,  $U_{a5}$  represents the upper marginal ray aperture angle of M5 on object side,  $h_{b6}$  represents the lower marginal ray height on M6, CL6 represents the longitudinal distance between the clear aperture of M6 and the upper marginal ray reflected from M5,  $z_{b6}$  represents the distance between the lower marginal ray incidence point on M6 and the vertex of M6, and  $z_{a5}$  represents the distance between the upper marginal incidence point on M5 and the vertex of M5. The parameter determination and design process of G3 are similar to that of G1. In this way, the initial design of G3 can be completed.

The middle group (G2) contains M3 and M4. Five configuration parameters of G2 should be figured out. They are the radius of M3 ( $r_3$ ), the radius of M4 ( $r_4$ ), the distance

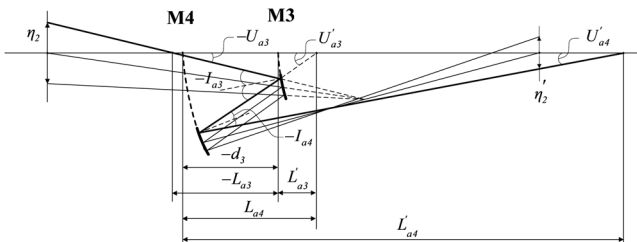


Fig. 5 Ray path of upper marginal ray in middle group.

between M3 and M4 ( $d_3$ ), the distance between the entrance pupil and M3 ( $L_{z3}$ ), and the distance between the exit pupil and M4 ( $L'_{z4}$ ). The layout of G2 is shown in Fig. 4.

G2 is designed to connect the ray path of G1 and G3. The entrance (exit) pupil of G2 should match the exit (entrance) pupil of G1 (G3) for both position and diameter. Thus the parameters of G2 should meet the real ray tracing equations. The ray path of chief ray in G2 is shown in Fig. 4. According to the ray path of the chief ray, we get

$$\begin{aligned} \sin I_{z3} &= \frac{L_{z3} - r_3}{r_3} \times \sin U_{z3} \\ U'_{z3} &= U_{z3} + 2I_{z3} \\ L'_{z3} &= r_3 \times \left( 1 - \frac{\sin I_{z3}}{\sin U'_{z3}} \right) \\ L_{z4} &= L'_{z3} - d_3 \\ \sin I_{z4} &= \frac{L_{z4} - r_4}{r_4} \times \sin U'_{z3} \\ U'_{z4} &= U'_{z3} + 2I_{z4} \\ L'_{z4} &= r_4 \times \left( 1 - \frac{\sin I_{z4}}{\sin U'_{z4}} \right), \end{aligned} \quad (8)$$

where  $I_{zi}$  represents the chief ray incidence angle on  $M_i$ ,  $U'_{zi}$  represents the chief ray aperture angle of  $M_i$  on image side,  $L_{zi}$  represents the intercept of the chief ray of  $M_i$  on the object side, and  $L'_{zi}$  represents the intercept of the chief ray of  $M_i$  on the image side.

The ray path of the upper marginal ray in G2 is shown in Fig. 5. According to the ray path of the upper marginal ray, we get

$$\begin{aligned} L_{a3} &= L_{z3} + \frac{\eta_2}{2 \times \tan U_{a3}} \\ \sin I_{a3} &= \frac{L_{a3} - r_3}{r_3} \times \sin U_{a3} \\ U'_{a3} &= U_{a3} + 2I_{a3} \\ L'_{a3} &= r_3 \times \left( 1 - \frac{\sin I_{a3}}{\sin U'_{a3}} \right) \\ L_{a4} &= L'_{a3} - d_3 \\ \sin I_{a4} &= \frac{L_{a4} - r_4}{r_4} \times \sin U'_{a3} \\ U'_{a4} &= U'_{a3} + 2I_{a4} \\ L'_{a4} &= r_4 \times \left( 1 - \frac{\sin I_{a4}}{\sin U'_{a4}} \right) \\ L'_{a4} &= L'_{z4} - \frac{\eta'_2}{2 \times \tan U'_{a4}}, \end{aligned} \quad (9)$$

where  $I_{ai}$  represents the upper marginal ray incidence angle on  $M_i$ ,  $U'_{ai}$  represents the upper marginal ray aperture angle of  $M_i$  on the image side,  $L_{ai}$  represents the intercept of the upper marginal ray of  $M_i$  on the object side, and  $L'_{ai}$  represents the intercept of the upper marginal ray of  $M_i$  on the image side.

In Eqs. (8) and (9),  $\eta_2$  ( $\eta'_2$ ) is the entrance (exit) pupil diameter of G2 which overlaps the exit (entrance) pupil of

G1 (G3) exactly,  $U_{z3}$  ( $U_{a3}$ ) is the chief (upper marginal) ray aperture angle of M3 on the object side, and  $U'_{z4}$  ( $U'_{a4}$ ) is the chief (upper marginal) ray aperture angle of M4 on the image side. These six parameters have been derived from G1 and G3. In addition, the petzval sum of the whole objective system should be zero to meet the aplanatic condition, so the radius  $r_3$  and  $r_4$  should satisfy the equation:

$$\frac{1}{r_3} - \frac{1}{r_4} = \left(-\frac{1}{r_1} + \frac{1}{r_2}\right) + \left(-\frac{1}{r_5} + \frac{1}{r_6}\right). \quad (10)$$

Equations (8), (9), and (10) are called conjugation constraints in which 17 independent equations and 17 variations are included. The five configuration parameters of G2 are contained in the 17 variations. So the five configuration parameters of G2 can be acquired by solving the conjugation Eqs. (8), (9), and (10). There may be many solutions of G2 because the conjugation equations are nonlinear. In this condition, the configuration of G2 with lower incidence angles on mirrors and free-obstruction will be chosen to connect G1 with G3 directly without an exhaustive search of variables and iterative computations. Then the grouping design for the spherical initial configuration of six-mirror objective is completed effectively.

If, unfortunately, the adequate solution of G2 with lower incidence angles on mirrors and free-obstruction does not exist, we have to modify a few parameters of G1 and G3 and redesign G2 until an adequate solution is acquired.

### 3 Generation of New Design Forms

The grouping design method with a real ray tracing model can be used to acquire different initial configurations

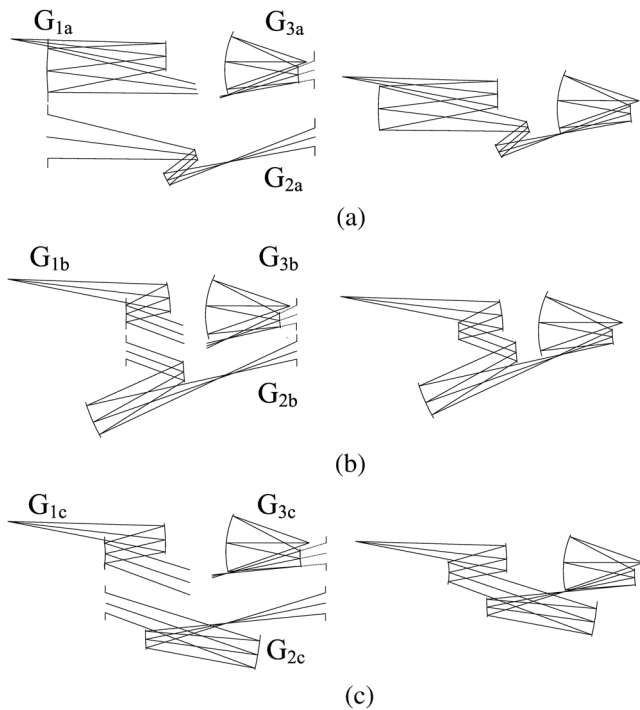


**Fig. 6** Initial configurations of the six-mirror objective with numerical aperture (NA) 0.33. (a) PPNPNP objective, (b) PNNPNP objective, and (c) PNPPNP objective (P denotes concave mirror and N denotes convex mirror).

of a high-NA objective. When the values of independent variables in G1 (G3) such as  $L_1$  ( $L_6$ ) and  $d_1$  ( $d_5$ ) are changed, a new design form of G1 (G3) can be calculated under the aperture stop constraint and nonobstruction constraint. To connect the ray path of the new G1 and G3, the potential design form of G2 would therefore change. A new initial configuration would be generated by connecting the three relative mirror groups. In this way, another two six-mirror objectives (NA 0.33) having the design forms illustrated in Figs. 6(b) and 6(c) were obtained.

In the design process of each mirror group, the beam incidence angle limitation is imposed to ensure that the design forms have lower incidence angles. This merit makes the three initial configurations perhaps more suitable for further optimization and compatible multilayer design compared with the initial configurations designed by the paraxial search method (see Figs. 7-9 in Appendix of Ref. 8). However, the diversity of the new design forms would be decreased due to the limitation imposed.

### 4 Objective Optimization and Performance

With the spherical initial configuration, aspheric coefficients must be added in the optimization process to achieve high-quality imaging performance. To keep the features of the initial configuration (low incidence angles on the mirrors and free-obstruction), an optimization process without changing ray paths too much is required. This is done by first optimizing the system with several low-order aspheric coefficient variables, then adding high-order aspheric coefficient variables and a perturbing operation gradually in the optimization process so that a minimum of merit function is acquired. The step of perturbations should be set properly since a too large step will make the final design far from the initial configuration.

With the design and optimization method mentioned above, a high-quality six-mirror objective system with an NA of 0.33 is obtained. The layout of the objective is shown in Fig. 7. The system specifications are shown in Table 1 and the optical characteristics are shown in Table 2. The total track is about 1360 mm and the back working distance is about 41 mm. The maximum aspheric departure is 40  $\mu\text{m}$  on M1. The incidence angles are well controlled and the chief ray angles of incidence are as follows: mask: 6.0 deg, M1: 6.3 deg, M2: 6.6 deg, M3: 22.4 deg, M4: 11.5 deg, M5: 12.4 deg, and M6: 4.7 deg. This objective has a composite RMS wavefront error 0.0258 $\lambda$  across a 26 mm  $\times$  1.5 mm ring field ( $R_0 = 34.75$  mm), and the distortions of all the field points are <0.8 nm. This design of a six-mirror objective provides a potential solution to 16-nm node of EUV lithography.

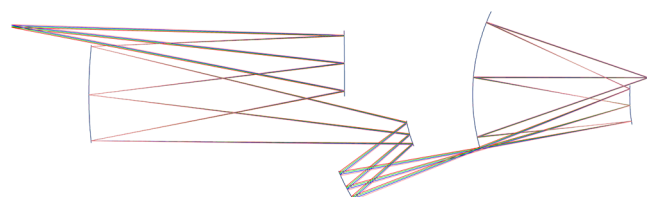


**Fig. 7** Layout of the NA 0.33 objective.

**Table 1** Lens prescription.

Surface	RDY	THI	GLA
OBJ	Infinity	715.29081	
1	-11128.1355	-554.79399	REFL
ASP			
K: 0	A: $8.08288 \times 10^{-10}$	B: $-7.10441 \times 10^{-15}$	C: $6.91406 \times 10^{-20}$
D: $-1.06125 \times 10^{-24}$	E: $3.98196 \times 10^{-29}$	F: $-1.47447 \times 10^{-33}$	G: $2.59527 \times 10^{-38}$
Stop	1066.82652	678.8141	REFL
ASP			
K: 0	A: $-4.43636 \times 10^{-11}$	B: $-1.66577 \times 10^{-16}$	C: $-4.04207 \times 10^{-21}$
D: $7.00735 \times 10^{-25}$	E: $-1.00950 \times 10^{-28}$	F: $7.18472 \times 10^{-33}$	G: $-2.04447 \times 10^{-37}$
3	287.84000	-168.29447	REFL
ASP			
K: 0	A: $-1.63326 \times 10^{-09}$	B: $2.43618 \times 10^{-14}$	C: $-5.90988 \times 10^{-18}$
D: $6.39116 \times 10^{-22}$	E: $-4.36016 \times 10^{-26}$	F: $1.67262 \times 10^{-30}$	G: $-2.79362 \times 10^{-35}$
4	412.72681	647.97319	REFL
ASP			
K: 0	A: $-3.41419 \times 10^{-11}$	B: $-3.02113 \times 10^{-16}$	C: $6.12747 \times 10^{-21}$
D: $2.97556 \times 10^{-25}$	E: $-1.54663 \times 10^{-29}$	F: $2.61783 \times 10^{-34}$	G: $-1.56288 \times 10^{-39}$
5	433.32378	-337.23112	REFL
ASP			
K: 0	A: $7.78766 \times 10^{-09}$	B: $4.78861 \times 10^{-13}$	C: $1.58479 \times 10^{-18}$
D: $7.93138 \times 10^{-22}$	E: $-2.28748 \times 10^{-25}$	F: $5.78703 \times 10^{-29}$	G: $-6.24238 \times 10^{-33}$
6	419.94362	377.79414	REFL
ASP			
K: 0.000000	A: $1.35823 \times 10^{-10}$	B: $9.60052 \times 10^{-16}$	C: $6.15294 \times 10^{-21}$
D: $-8.00149 \times 10^{-28}$	E: $2.50766 \times 10^{-30}$	F: $-7.16751 \times 10^{-35}$	G: $9.17681 \times 10^{-40}$
IMG	INFINITY	0	

## 5 Conclusions

We have presented a grouping design method using a real ray tracing model for EUV lithographic objectives. An example of an NA 0.33 EUV objective design has demonstrated some advantages of this method. Some real ray constraints (aperture stop constraint, nonobstruction constraint, conjugation constraint) are imposed on the three mirror groups' design,

which makes the independent variables reduced from 13 to only 4 in a spherical initial six-mirror system. In the meantime, real ray tracing avoids the discrepancy of ray path and the pupils mismatch of groups which are caused by paraxial approximation. Thus, the three mirror groups can be connected directly without an exhaustive search of variables and iterative calculations. The merits of this method mentioned

**Table 2** Optical characteristics.

Wavelength	13.5 nm
Numerical aperture	0.33
Image-side field of view	26 mm × 1.5 mm
Magnification	0.25
Total track length	1360 mm
Back working distance	41 mm
Chief ray angle of incidence on mask	6 deg
Telecentricity on wafer	0.02 deg
Wavefront error (RMS)	0.0258 $\lambda$
Max distortion	0.8 nm
Order of aspheric coefficient	16th
Max aspheric departure	40 $\mu\text{m}$

above improve the efficiency of the design process. Furthermore, we control the incidence angles on reflective mirrors in the design process which makes initial configurations suitable for further optimization and compatible multi-layer designs. These advantages enable an optical designer to get an initial and qualified high-NA EUV objective effectively in a short time.

### Acknowledgments

We thank the financial support by the National Science and Technology Major Project.

### References

1. W. Ulrich, S. Beiersdorfer, and H. J. Mann, "Trends in optical design of projection lens for UV and EUV lithography," *Proc. SPIE* **4146**, 21–23 (2000).
2. O. Marinescu and F. Bociort, "Optimization of extreme ultraviolet mirror systems comprising high-order aspheric surfaces," *Opt. Eng.* **47**(3), 033004 (2008).
3. J. Chang et al., "All-reflective optical system design for extreme ultraviolet lithography," *Chin. Opt. Lett.* **8**(11), 1082–1084 (2010).

4. M. Lowisch et al., "Optics for EUV production," *Proc. SPIE* **7636**, 763603 (2010).
5. D. Chan and S. Gmuend, "Projection objectives having mirror elements with reflective coating," U.S. Patent No. 8,194,230 (2012).
6. S. A. Lerner, J. M. Sasian, and M. R. Descour, "Design approach and comparison of projection cameras for EUV lithography," *Opt. Eng.* **39**(3), 792–796 (2000).
7. M. F. Bal, F. Bociort, and J. J. M. Braat, "Analysis, search, and classification for reflective ring-field projection systems," *Appl. Opt.* **42**(13), 2301–2309 (2003).
8. F. Bociort, M. F. Bal, and J. J. M. Braat, "Systematic analysis of unobscured mirror systems for microlithography," *Proc. ODF*, Vol. 2, 339–342 (2000).
9. R. Hudyma, "High numerical aperture ring field projection system for extreme ultraviolet lithography," U.S. Patent No. 6,033,079 (2000).
10. F. Liu and Y. Li, "Design of multi-mirror optics for industrial extreme ultraviolet lithography," *Opt. Rev.* **20**(2), 121–126 (2013).
11. F. Liu and Y. Li, "Grouping design of eight-mirror projection objective for high-numerical aperture EUV lithography," *Appl. Opt.* **52**(29), 7137–7144 (2013).
12. V. Bakshi, "EUV lithography," Chapter 4B in *The Projection Systems for Extreme Ultraviolet Lithography*, R. M. Hudyma and R. Soufli, Eds., pp. 135–138, SPIE, Bellingham, WA (2008).
13. J. T. Neumann et al., "Interactions of 3D mask effects and NA in EUV lithography," *Proc. SPIE* **8522**, 852211 (2012).



**Zhen Cao** received the BS degree in optoelectronic information engineering from Xi'an Technological University in 2008. He is currently a PhD candidate directed by Professor Yanqiu Li in the School of Optoelectronics at Beijing Institute of Technology. His current interests include optical system design for EUVL.



**Yanqiu Li** received the MS and PhD degrees in optics from Harbin Institute of Technology. She worked as a director of the micro- and nanofabrication division at Institute of Electrical Engineering Chinese Academy of Science, as a senior engineer at Nikon, as an invited professor of Tohoku University of Japan, and as a frontier researcher at RIKEN of Japan. She is currently a professor of School of Optoelectronics at Beijing Institute of Technology, Beijing, China.

**Fei Liu** received the BS degree in measurement and control technology and instruments from Changchun University of Science and Technology in 2008. She is currently a PhD candidate directed by Professor Yanqiu Li in the School of Optoelectronics at Beijing Institute of Technology. Her current interests include optical system design for EUVL.